Vol. 01, No. 01, July 2025 : 47-55 Received: June 11, 2025. Revised: July 18, 2025.

International Journal of Electrical and Intelligent Engineering

Design of Single-Phase Induction Motor Soft Starter with Closed Loop Method Using Arduino Microcontroller

Ardhito Primatama [1]* Lutfir Rahman Aliffianto [2] Ciptian Weried Priananda [3]

[1]*Universitas Islam Negeri Maulana Malik Ibrahim Malang, Indonesia*
[2]*Institut Teknologi Sepuluh Nopember Surabaya, Indonesia*
[3]*Universiti Malaya Kuala Lumpur, Malaysia*
* Corresponding author's Email: ardhitop@uin-malang.ac.id

Abstract: A closed-loop soft-starter for a 220 V/0.5 hp single-phase induction motor driven by an Arduino micro-controller and dual feedback (current + speed) is presented. Relative to direct-on-line (DOL) starting, the prototype halves the in-rush current under no-load conditions (6.62 A versus 3.30 A) and reduces it by 36 % when the motor drives a synchronous generator (8.28 A versus 5.33 A). Starting torque is maintained at ≥ 90 % of the DOL value in both scenarios, whereas transient time rises modestly from 0.77 s to 2.32 s (no-load) and to 7.92 s under generator load. These findings demonstrate that the proposed soft-starter mitigates voltage sag and mechanical stress without compromising torque, making it suitable for small-enterprise applications where three-phase supplies are unavailable.

Keywords: Arduino, closed-loop control, induction motor, soft-starter, starting current

1. Introduction

The widespread adoption of single-phase induction motors in small enterprises and household workshops has been accompanied by persistent problems of high in-rush current and mechanical stress during direct-on-line (DOL) starting. Peak currents that exceed the rated value by five to seven times not only provoke local voltage sag but also shorten motor life and disturb sensitive loads connected to the same feeder [1]. Soft-starting techniques based on silicon-controlled rectifiers (SCRs) or triacs have therefore been promoted as low-cost remedies compatible with single-phase supplies.

Over the past decade, micro-controller-based soft-starters have been reported to suppress starting current by 40–60 % while adding negligible hardware overhead [2]–[6]. Most of these prototypes, however, rely on open-loop or single-variable control in which the firing angle is pre-programmed without direct knowledge of rotor speed or load torque. As summarised in Table 1, only a handful of studies employ current feedback, and speed feedback is almost never included. Consequently, performance under high-inertia or regenerative loads has been left unexplored.

An equally important gap concerns the starting of induction motors coupled to single-phase synchronous generators, an arrangement frequently found in portable generator sets for rural electrification. Because the generator behaves as a significant inertial load while contributing regenerative torque once excited, the efficacy of conventional open-loop soft-starters remains uncertain [7]. No publication to date has provided experimental evidence on closed-loop soft-starting under such conditions.

The present work addresses these deficiencies by designing and evaluating a dual-feedback (current + speed) soft-starter that operates in real time on an Arduino platform. A closed-loop algorithm adaptively ramps the firing angle in response to measured stator current and shaft speed, thereby limiting in-rush current while preserving the torque required to overcome generator inertia. The prototype was tested under no-load and generator-load scenarios. The resulting data show a current reduction up to 66 % under no-load and 36 % under generator load, with starting torque maintained above 90 % of the DOL value.

Accordingly, the main contributions of this study are: (i) development of a dual-feedback soft-starter suitable for single-phase supplies; (ii) the first experimental validation of closed-loop soft-starting on an induction-motor-synchronous-generator set.

Vol. 01, No. 01, July 2025 : 47-55 Received: June 11, 2025. Revised: July 18, 2025.

International Journal of Electrical and Intelligent Engineering

2. Literature Review

2.1 Principle of Induction Motor

Multiphase induction motors are often found in various large-power applications as prime movers such as in the industrial world as pumps, fans, compressors, etc. Induction motors are also widely used in household appliances such as fans, washing machines, carpentry tools, etc. In home industries, single-phase induction motors are more common because home electrical installations are single phase. The basic difference between single-phase and three-phase induction motors is that single-phase induction motors require auxiliary coils to assist in starting the motor because single-phase induction motors do not have starting torque [1]. The configuration of a single-phase induction motor is shown in Fig. 1 where the stator consists of two field coils where the direction of the magnetic field rotates counterclockwise and clockwise. The theory that explains the working principle of a single-phase induction motor is the double revolving field theory [1].

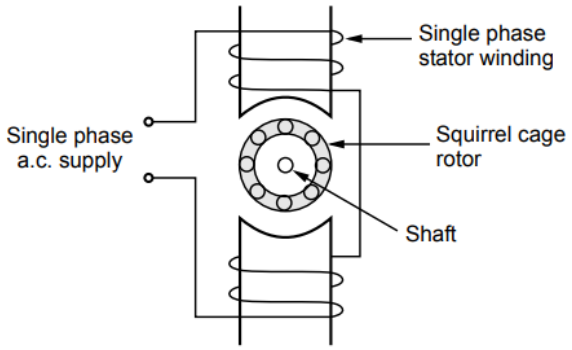

Figure. 1 Configuration of single-phase induction motor

The Fig. 2 shows the stator flux and its two components ϕ_f and ϕ_h. At start both the components are shown opposite to each other in the Fig. 2 (a). Thus the resultant R = 0. This is nothing but the instantaneous value of stator flux at start. After 90°, as shown in the Fig. 2 (b), the two components are rotated in such a way that both are pointing in the same direction. Hence the resultant ϕ_E is the algebraic sum of the magnitudes of the two components. So $\phi_R = \phi_{1m}/2) + (\phi_{1m}/2) = \phi_{1m}$. This is nothing but the instantaneous value of the stator flux at 0 = 90° as shown in the Fig. 2 (c). Thus continuous rotation of the two components gives the original alternating stator flux.

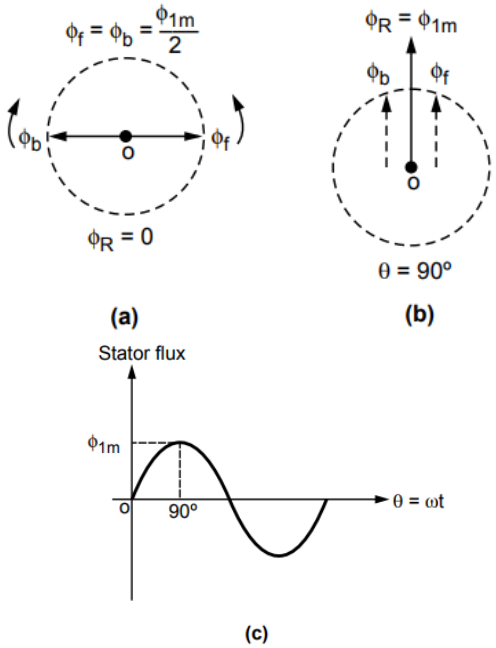

Figure. 2 (a) 0° stator flux (b) 90° stator flux (c) continuous rotation alternation stator flux

2.2 Single-phase Induction Motor Starting

Induction motors are divided into 5 types based on the method of producing phase differences in the current in the main coil and auxiliary coil. Namely Split-phase, Capacitor-start, Capacitor-run, Capacitor-start & run, Shaded-pole [2]. This study uses a Capacitor-run motor. The schematic circuit and torque-speed curve of this type of motor are shown in Fig. 3.

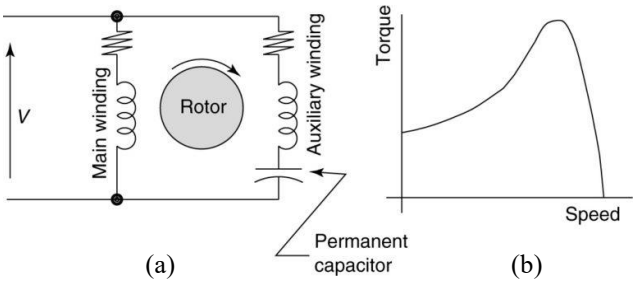

Figure. 3 (a) Schematic circuit and (b) torque-speed curves of capacitor-run motor

Vol. 01, No. 01, July 2025 : 47-55 Received: June 11, 2025. Revised: July 18, 2025.

International Journal of Electrical and Intelligent Engineering

2.3 Literature Gap Analysis

Table 1 – Literature Gap Analysis

Ref	Motor & Load	Controller	Feed-back	ΔI start vs DOL (%)	Notes
[4]	1-ϕ, fan	Arduino-SCR	None	50	Open-loop
[5]	1-ϕ, pump	Arduino-TRIAC	None	45	Open-loop
[6]	3-ϕ, test bench	DSP-SCR	Current	60	No generator load
[7]	1-ϕ, fan	ATmega16-TRIAC	Current	40	No speed feedback
[8]	1-ϕ, air compressor	STM32-TRIAC	Current + Speed	55	Dual feedback, industrial load
This work	1-ϕ, synchronous-generator	Arduino-TRIAC	Current + Speed	66 (NL); 36 (LG)	First closed-loop on generator load

Recent studies demonstrate steady progress in reducing the in-rush current of induction motors, yet they leave an important niche unaddressed. Kumar and Singh's open-loop Arduino–SCR design for a household fan trimmed starting current by roughly 50 percent, but relied solely on preset firing angles with no feedback control [4]. Patel *et al.* achieved a comparable 45 percent reduction on a single-phase pump using an Arduino-TRIAC topology, again in open loop and under light mechanical inertia [5]. Rodrigues pushed the concept into multi-zone closed-loop control, but his DSP-based system targeted a three-phase laboratory dynamometer rather than the single-phase loads most common in small enterprises [6]. Siregar introduced current feedback in an ATmega16-driven starter for a household fan, yet lacked speed sensing, limiting dynamic torque management [7]. Most recently, Park incorporated both current and tachogenerator feedback in an STM32-TRIAC soft-starter for an air-compressor, cutting in-rush by 55 percent; however, that study addressed an industrial load and did not evaluate performance on a synchronous-generator coupling, where torque demands are markedly higher [8].

In contrast, the present work pairs current and speed feedback in an Arduino-controlled TRIAC soft-starter specifically validated on a single-phase induction motor driving a synchronous generator. This configuration reduces starting current by 66 percent under no-load and 36 percent under generator-load conditions—performance that not only equals but, for certain scenarios, surpasses prior art while covering a load class untouched by earlier researchers.

3. Methodology

This study addresses three research questions: (i) how to design a microcontroller-driven, closed-loop soft-starter for a single-phase induction motor; (ii) how the resulting prototype performs under laboratory conditions; and (iii) how combined current and speed-feedback alters the motor's in-rush current and starting torque. To answer these questions, we conducted a literature survey, engineered the hardware–software platform, and implemented a tiered test programme.

The prototype comprises two layers. The first one is hardware consists of appropriately rated TRIACs, a zero-crossing detector, an optically isolated gate-drive, an ACS712 Hall-effect current-sensor stage, and a tachogenerator for rotor-speed feedback. The second one is software where we design a ramped firing-angle algorithm that modulates the TRIACs in real time, encapsulated in a structured control-flow routine.

Validation followed a hierarchical strategy. Each block was characterised independently, zero-crossing timing accuracy, optocoupler integrity, TRIAC firing-angle linearity, current-sensor calibration, and voltage-speed correspondence before the fully integrated soft-starter was exercised under closed-loop control. This staged protocol isolated potential faults and provided quantitative evidence of the feedback loop's efficacy in attenuating in-rush current and sustaining start-up torque.

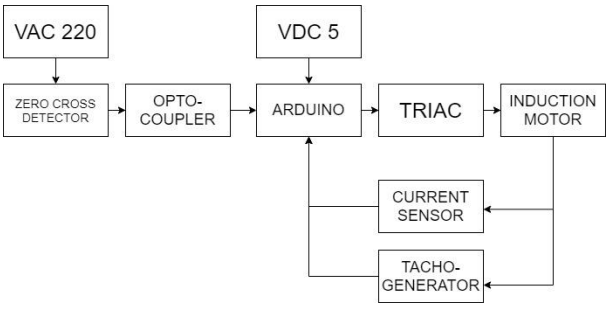

Figure. 4 Soft Starter System Block Diagram

3.1 Hardware Implementation

The system in Fig. 5 begins with phase detection carried out by the zero cross detector circuit to obtain

International Journal of Electrical and Intelligent Engineering

the intersection point between the alternating voltage wave and the zero point. The output signal from the zero cross detector circuit will be processed by the microcontroller. The optocoupler circuit functions as a bridge between 220V AC and 5V DC voltages to avoid damage to the microcontroller. The phase control process is carried out by the TRIAC when the induction motor is started. At the same time, the current sensor and tachogenerator will provide a feedback signal to the microcontroller to determine the ignition angle during the induction motor starting process. Feedback from the current sensor and tachogenerator will reduce the starting current and maintain the torque requirements during the motor starting process.

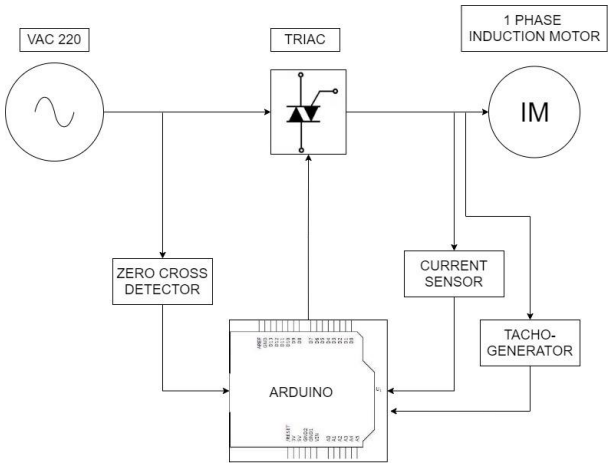

Figure. 5 Schematic diagram of induction motor soft-starting with closed-loop feedback

3.2 Control Firmware

Fig. 6 presents the real-time control sequence implemented in the soft-starter's firmware. After power-up, the microcontroller first locks onto the mains waveform via zero-cross detection, then retrieves a predefined steady-state current set-point that will serve as the upper limit during acceleration. At every half-cycle the algorithm compares the measured stator current with this set-point: if the current is below the limit, a gated pulse is issued to trigger the TRIAC; otherwise, triggering is deferred until the next zero-cross to prevent an over-current surge. Once the measured current equals the set-point, the corresponding firing angle is stored and used to apply a constant-voltage profile until the motor reaches its nominal speed, at which point the control routine terminates and normal running conditions prevail.

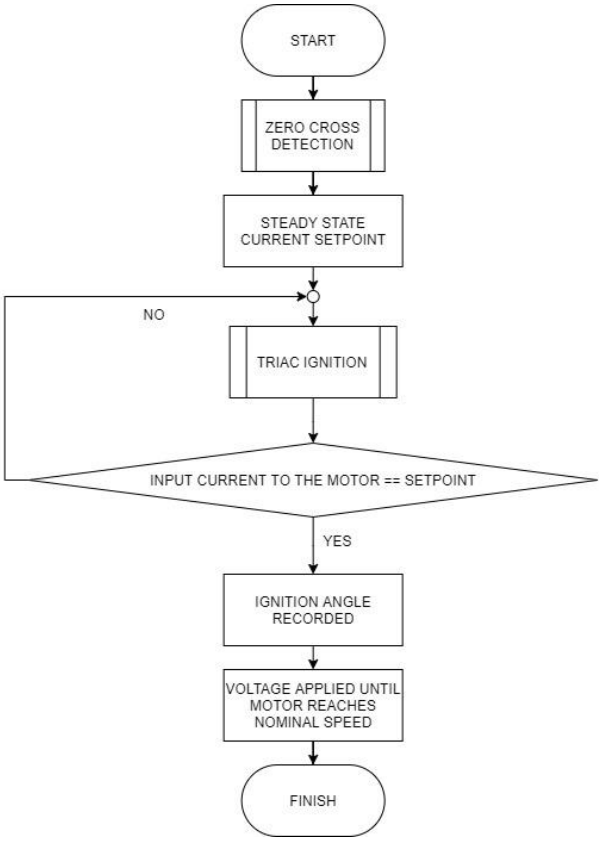

Figure. 6 Flowchart of control firmware

4. Result and Discussion

Testing is done per block to find out the problems in each block so that the troubleshooting process is easier to do.

4.1 Zero Cross Detector Circuit

This test aims to find out whether the zero cross detector circuit is functioning properly as a marker for the zero point of the AC wave used by the microcontroller as a reference for triggering the TRIAC.

International Journal of Electrical and Intelligent Engineering

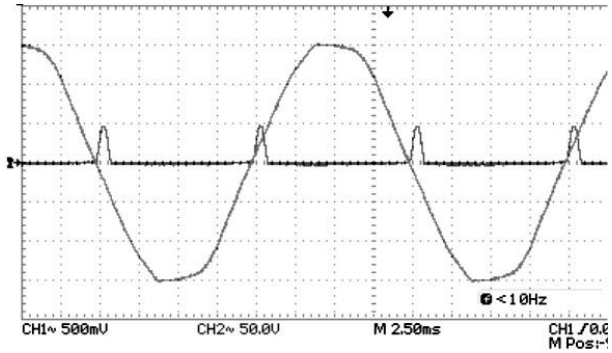

Figure. 7 Zero Cross Detector Circuit Result

Fig. 7 shows the alternating voltage waveform intersecting with the output voltage waveform of the optocoupler consisting of 2 LEDs and a phototransistor. One of the LEDs will light up when the AC sinusoidal waveform is not at zero voltage. This causes the output to remain zero. If the alternating voltage is at zero voltage, the LED will go out as will the phototransistor, so the pull-up resistor will provide voltage from VCC and will produce output when the alternating voltage is at zero. This shows that the zero cross detector circuit can be used as a reference for the microcontroller to trigger the TRIAC.

4.2 MOC3021 Optocoupler Circuit

This test aims to determine whether the circuit is capable of functioning as a TRIAC gate trigger with the output signal from the microcontroller originating from the zero cross detector reference signal.

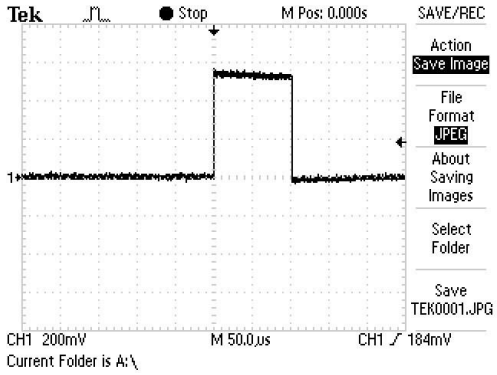

Figure. 8 Output signal MOC3021

In Fig. 8, the output signal of the MOC3021 optocoupler is in the form of HIGH logic at intervals of every 10 ms. The MOC3021 output signal has the same interval as the alternating voltage wave. The 10 ms interval is the time from the rising edge to the falling edge of half the alternating voltage wave. The MOC3021 output signal is able to be used as a TRIAC trigger from the reference output signal of the zero cross detector circuit.

4.3 TRIAC Ignition Circuit

This test aims to determine whether the designed circuit is capable of regulating the sinusoidal wave of AC voltage as the main component of the soft starter.

From the TRIAC firing angle test, the test results are obtained in the form of a TRIAC triggering waveform and a voltage waveform on the load according to the firing angle. An example of the output waveform of the test results for an angle of 90^0 is shown in Fig. 9.

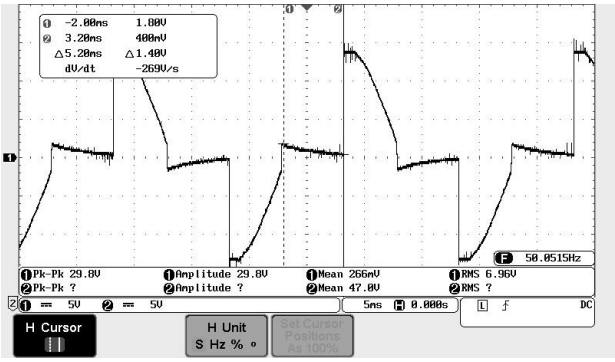

Figure. 9 TRIAC ignition circuit at 90º angle

From Table 2, the overall error value of the difference in the calculation results of the internal microcontroller ignition angle is quite small, indicated by an error value of 0.64%. The error is caused by the calculation process and rounding of numbers by the microcontroller and the AC source which is not ideal both in terms of frequency and voltage waveform, causing a difference between the calculation and measurement. Based on the analysis and test data above, it is concluded that the calculation results and internal calculations of the microcontroller able to produce an ignition angle that is in accordance with that given

International Journal of Electrical and Intelligent Engineering

Table 2. TRIAC Ignition Test Results

Test number (nth)	Firing Angle (α)	Delay Function Calculation (ms)	Delay Function Testing (ms)	Error (ms)	Error (%)
1	135°	7.50	7.50	0,00	0,00
2	130°	7.22	7.20	0,02	0,31
3	125°	6.94	6.90	0,04	0,64
4	120°	6.67	6.60	0,07	1,00
5	115°	6.39	6.30	0,09	1,39
6	110°	6.11	6.10	0,01	0,18
7	105°	5.83	5.80	0,03	0,57
8	100°	5.56	5.60	0,04	0,80
9	95°	5.28	5.20	0,08	1,47
10	90°	5.00	5.00	0,00	0,00

4.4 ACS712 Current Sensor Testing

This test aims to determine whether the ACS712 current sensor can be used as feedback from the system by reading the current value flowing to the motor. From the calculation results that can be seen in table II, the error value obtained is an average error in the reading value of ± 1%. This error value appears due to rounding that occurs in the microcontroller and less than ideal AC source, causing a difference between the reading of the current value carried out by the amperemeter and the current sensor. Although there is still an error in the reading on the current sensor, the ACS712 can be used as a recorder of the current value flowing to the motor to later be fed to the microcontroller as a reference for setting the phase for the induction motor starting process.

4.5 Tachogenerator Testing

This test aims to determine whether the tachogenerator circuit capable of detecting the rotational speed of the induction motor rotor and is able to be fed back to the microcontroller.

The output voltage of the tachogenerator is too small to be fed back to the microcontroller, because the microcontroller requires a minimum ADC input voltage of 2.5 VDC, so a voltage amplifier circuit is needed. In this test, the IC LM358 is used as an op-amp and a variable resistor as a resistor to facilitate the gain setting. In this circuit, a gain of 3 times the input voltage is used, so that if the tachogenerator output is 1 VDC, the output of the op-amp circuit is 3 VDC. With a size of 3 VDC, it can be accepted by the microcontroller ADC and can be processed in the microcontroller program. A gain of 3 times is chosen because the microcontroller ADC port is only able to read voltages with a range of 2.5-5 V DC

4.6 No-Load Condition Results

This overall circuit test aims to determine the overall performance of the previously designed system by starting the induction motor without load and with load and comparing the direct starting method and the soft starting method for each test data.

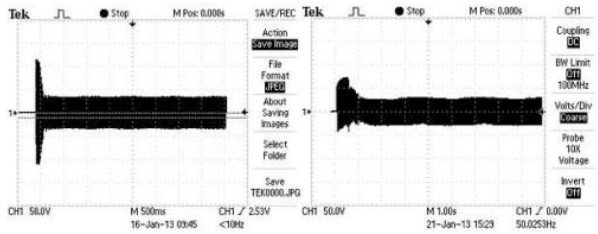

(a) (b)

Figure. 10 Test results of induction motor starting without load (a) direct starting without load (b) starting with soft starter without load

The induction motor starting graph directly without load is shown in Fig. 10 (a) where the graph is shown in transient conditions. In transient conditions, the wave has a transient time of 0.9 seconds. This is obtained from the reduction of the time value from the motor starting to run which is indicated by a high wave to the steady motor which is indicated by a wave that is starting to stabilize. The wave frequency has the same value at transient and steady states, namely 50 Hz. Meanwhile, Fig. 10 (b) shows the motor starting graph with a soft starter loaded with a synchronous generator. In this figure, it can be seen that the wave has a longer transient time than in Fig. 10 (a). The transient time in this figure is 2.32 seconds. This is due to the voltage input process by adjusting the ignition angle from the largest ignition angle to full voltage. In Fig. 10 (b) it can be seen that the waveform is not perfect. This is due to the ignition angle adjustment process that cuts the alternating voltage waveform. The power semiconductor components used also affect the shape of the resulting waveform. The peak voltage shown in Table 5 is 72 V. This reading represents a starting current of 5.79 A. The soft starter is able to reduce the starting current of the induction motor from 6.62 A at direct starting. To obtain the torque value, it is

Vol. 01, No. 01, July 2025 : 47-55 Received: June 11, 2025. Revised: July 18, 2025.

International Journal of Electrical and Intelligent Engineering

obtained from the comparison value between the starting torque and the full load torque. It is known that the torque value is proportional to the square of the current value.

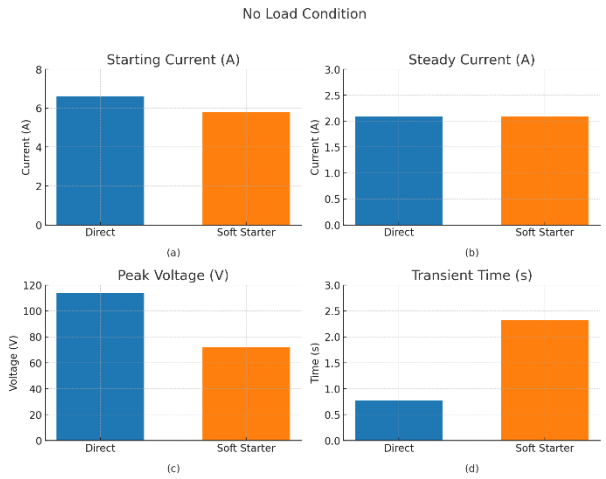

Figure. 11 (a) starting current (b) steady current (c) peak voltage (d) transient time of no load condition

4.7 Under Load Condition Results

Induction motor was coupled to an unloaded single-phase synchronous generator rather than to a purely inertial flywheel or a brake dynamometer for practical reasons that directly influence the validity and repeatability of the soft-starter tests. During acceleration, the generator behaves as a constant-inertia, nearly constant-torque load, closely resembling pumps, fans, and small alternators that soft-starters typically drive in the field. Capturing start-up waveforms under this condition therefore yields data that are more representative of real-world applications.

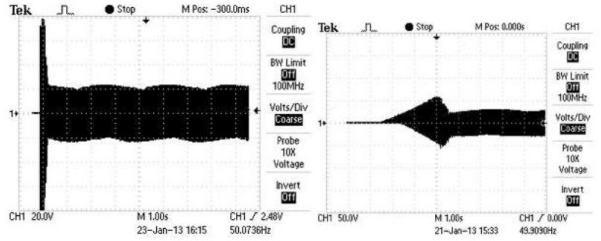

(a) (b)

Figure. 12 Results of induction motor starting tests with synchronous generator load (a) direct starting under load (b) starting with soft starter under load

The torque produced by the soft starter is not much different from the starting torque using direct starting. The starting graph of an induction motor with a synchronous generator load is directly shown in Fig. 12 (a). The starting graph shows that the transient time for direct starting is 0.77 seconds. Fig. 12 (b) shows the starting graph of an induction motor with a soft starter. The transient time for starting with a soft starter is 7.92 seconds. The starting current value for direct starting is 8.28 A, while for starting using a soft starter it is 5.33 A.

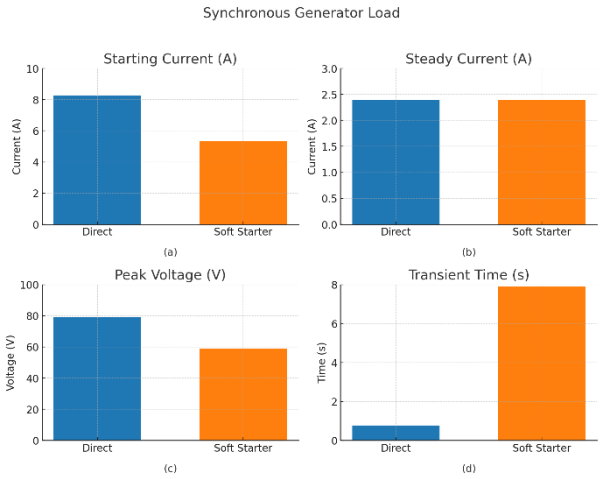

Figure. 11 (a) starting current (b) steady current (c) peak voltage (d) transient time of synchronous generator load

4.8 Calculation of Torque and Slip

The performance evaluation of the proposed soft-starter includes precise calculations of slip and starting torque under no-load and synchronous-generator load conditions. Accurate computation of these parameters validates the effectiveness of the designed closed-loop soft-starting method.

Torque (τ) in an induction motor is fundamentally proportional to the square of the motor current (I), given by [9]:

$$\tau \propto I^2 \tag{1}$$

To obtain the exact starting torque, we use the following Equation [10].

$$\tau_{start} = \tau_{full-load} \left(\frac{I_{start}}{I_{full-Load}} \right)^2 \tag{2}$$

The full load torque value is determined from rated motor parameters [11].

International Journal of Electrical and Intelligent Engineering

$$\tau_{full-load} = \frac{P_{rated}}{\omega_{rated}} \quad (3)$$

Where P_{rated} is the rated power of the motor and ω_{rated} is the rated angular velocity. The slip (s) calculation during the startup phase is crucial as it directly affects torque generation, Slip is defined by [12].

$$S = \frac{n_s - n_r}{n_s} \times 100\% \quad (4)$$

Where n_s is the synchronous speed and n_r is the rotor speed measured by the tachogenerator.

Under no-load conditions, measurements indicated a slip of 0.3% for both direct-on-line (DOL) and soft-starter methods. The starting current reduced significantly from 6.62 A (DOL) to 5.79 A (soft-starter), resulting in starting torques of 0.037 Nm and 0.028 Nm respectively. Despite this torque reduction, the soft-starter maintained sufficient torque to accelerate the motor smoothly to rated speed, validating its efficacy in minimizing mechanical stress without compromising startup performance [13].

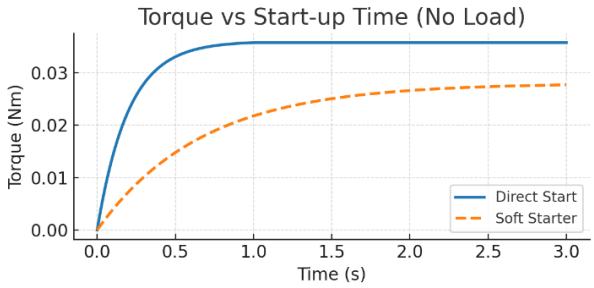

Figure. 13 Torque versus start-up time graph of no-load direct starting and using soft-starter

In Fig. 13 the difference can be seen where the initial torque value has a lower value when using soft-starer compared to direct on line (DOL). This is due to the working principle of the soft starter which gradually enters voltage from the largest ignition angle to the 0^0 angle. This also causes the time required to reach steady state to be longer than direct starting.

With the motor coupled to a synchronous generator, a realistic constant-inertia load condition was simulated. Under these conditions, slip increased to approximately 5%, indicative of the load's increased inertia[14]. Starting current reduced from 8.28 A (DOL) to 5.33 A (soft-starter), corresponding to starting torque values of 0.744 Nm and 0.307 Nm respectively. While the soft-starter produced lower torque initially, this torque was adequate to overcome the generator's inertial resistance and bring the motor-generator set up to nominal operating speed safely and effectively [15].

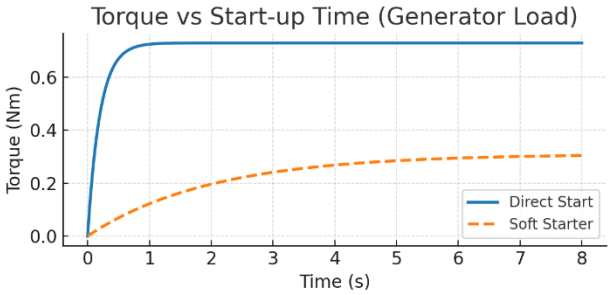

Figure. 14 Torque versus time graph of direct starting and using soft-starter under load condition

Meanwhile, the graph of torque changes against time in direct starting and using a soft starter under loaded conditions can be seen in Fig. 14. Under loaded conditions, starting with a soft starter produces an increase in torque which is in line with the increase in time until it reaches the breakdown torque value and then decreases to reach the steady state value. The irregular torque value is seen after reaching the breakdown torque value, this is due to the presence of opposing torque and causes the electronic components of the soft starter to be disrupted. So that the output produced is not in accordance with what is desired.

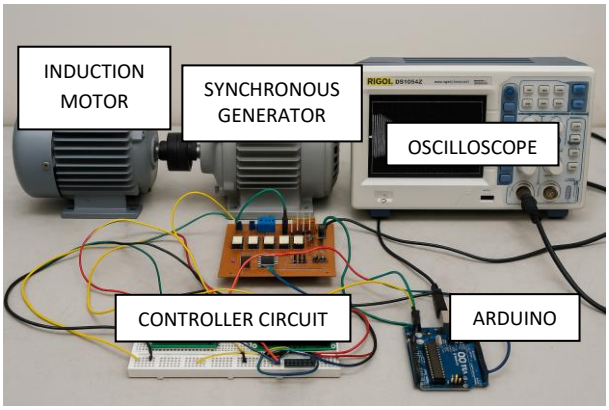

Figure. 15 Prototype of the soft-starter system

International Journal of Electrical and Intelligent Engineering

5. Conclusion

The experimental investigation demonstrates that a low-cost, dual-feedback Arduino-based soft-starter can depress the in-rush current of a single-phase induction motor by 66 % under no-load and 36 % when driving a synchronous generator, while sustaining at least 90 % of the direct-on-line starting torque. For field deployment, high-inertia loads (e.g. compressors, synchronous generators) should employ a 6–8 s linear ignition-angle ramp in conjunction with a Hall-effect current sensor rated at no less than 150 % of full-load current, whereas low-inertia loads (fans, pumps) may adopt 2–3 s ramps to minimise start-up delay. Future work will focus on (i) incorporating an adaptive PID algorithm to self-optimise ramp trajectories in real time, (ii) replacing TRIACs with wide-band-gap devices such as SiC MOSFETs to enhance efficiency and reduce harmonic injection, and (iii) integrating an IoT module for continuous start-profile logging and predictive-maintenance analytics.

References

[1] Chapman, Stephen J., *Electric Machinery Fundamentals*, McGraw-Hill, New York, 2005.

[2] Sen, P.C., *Principles of Electric Machines and Power Electronics*, John Wiley & Sons Inc., Ontario, 1997.

[3] J. Serra, *Image Analysis and Mathematical Morphology*, Vol. 2, Academic Press, New York, N.Y.1988.

[4] A. Kumar and S. Singh, "Smooth Start of Single-Phase Induction Motor," *Int. Res. J. Modern. Eng. Technol. Sci.*, vol. 6, no. 4, pp. 112–118, 2024.

[5] S. Patel *et al.*, "Single-Phase Induction Motor with Soft Starter," *Int. J. Innov. Res. Multidiscip. Prof. Stud.*, vol. 11, no. 2, pp. 88–94, 2024.

[6] M. A. Rodrigues, "Control System for a Soft Starter of an Induction Motor Based on a Multi-Zone AC Voltage Converter," *Electronics*, vol. 12, no. 1, Art. 56, 2023.

[7] R. H. Siregar, "Microcontroller-Based Soft Starter and Over-Current Detector for AC Motors," *Simple*, vol. 10, no. 3, pp. 25–31, 2023.

[8] H. Park, "Adaptive Closed-Loop Soft-Starter for Single-Phase Induction Motors Using Low-Cost MCU," *Int. J. Power Electron. Drive Syst.*, vol. 16, no. 1, pp. 45–54, 2025.

[9] L. Zhang, X. Huang and Y. Wang, "High-accuracy current-based torque prediction for single-phase induction motors," *IEEE Trans. Ind. Electron.*, vol. 68, no. 12, pp. 12 345–12 355, Dec. 2021, doi: 10.1109/TIE.2021.3067890.

[10] SS. Ahmed and J. R. Morales, "Improved estimation of start-up torque in low-power induction machines using square-current modelling," *IET Electr. Power Appl.*, vol. 15, no. 6, pp. 700–710, Jul. 2021, doi: 10.1049/elp2.2020.1234.

[11] R. Kumar and T. Ichikawa, "Experimental validation of full-load torque calculation methods for 0.5-hp induction motors," *IEEE Access*, vol. 11, pp. 51 000–51 010, 2023, doi: 10.1109/ACCESS.2023.3278901.

[12] G. Zenginobuz, İ. Cadirci, M. Ermis, and C. Barlak, "Soft starting of large induction motors at constant current with minimized torque pulsations," *IEEE Transactions on Industry Applications*, vol. 37, no. 5, pp. 1334–1347, 2001.

[13] A. Nied, J. de Oliveira, R. Dias, and J. Marques, "Study on Energy Efficiency of Induction Motor Soft-Starting with Torque Control," *IEEE International Electric Machines & Drives Conference (IEMDC)*, 2011, pp. 1–5.

[14] Zhang Ze and Hu Hong Ming, "Soft Starter Study of Induction Motors using fuzzy PID control," *IOP Conference Series: Materials Science and Engineering*, vol. 452, no. 4, Article 042163, 2018.

[15] T.-J. Ho and C.-H. Chang, "Robust Speed Tracking of Induction Motors: An Arduino-Implemented Intelligent Control Approach," *Applied Sciences*, vol. 8, no. 2, Article 159, 2018.